

Single-molecule Protein Phosphorylation and Dephosphorylation by Nanopore Enzymology

Leon Harrington^{1,†,}, Leila T. Alexander^{2,‡}, Stefan Knapp^{2,§} and Hagan Bayley^{1,*}*

¹Department of Chemistry, University of Oxford, 12 Mansfield Road, Oxford, OX1 3TA, United Kingdom

²Nuffield Department of Clinical Medicine, Structural Genomics Consortium and Target Discovery Institute, University of Oxford, Oxford, OX3 7DQ, United Kingdom

KEYWORDS: nanopore enzymology, phosphorylation, protein kinases, single-molecule, kinase mechanism, metal ions

ABSTRACT: Reversible protein phosphorylation plays a crucial and ubiquitous role in the control of almost all cellular processes. The interplay of protein kinases and phosphatases acting in opposition ensures tight dynamic control of protein phosphorylation states within the cell. Previously, engineered alpha-hemolysin pores bearing kinase substrate peptides have been developed as single-molecule stochastic sensors for protein kinases. Here, we have used these pores to observe, label-free, the phosphorylation and dephosphorylation of a single substrate molecule. Further, we investigated the effect of Mg^{2+} and Mn^{2+} upon substrate and product binding and found that Mn^{2+} relaxes active site specificity towards nucleotides and enhances

product binding. In doing so, we demonstrate the power and versatility of nanopore enzymology to scrutinise a critical post-translational modification.

Engineered nanopores are now well established as powerful tools for the single-molecule detection and analysis of a wide range of molecules.^{1, 2} Most prominently, there has been a long and extensive effort focused on the sensing of polynucleotides,³ culminating in a commercialized device for direct sequencing of DNA,⁴ and recently, RNA.⁵ More recently, attention has turned to the relatively more complex problem of protein sensing. Applications include the monitoring of protein unfolding,^{6, 7} and detection of post-translational modifications.^{8, 9} Further, nanopores have been used to follow enzyme activity by the detection of products,¹⁰⁻¹⁴ as well as the processing of polymeric substrates such as DNA by processive enzymes.^{15, 16} Synthetic nanopores have also been extensively used for protein detection, although they are harder to engineer.^{17, 18} With the adoption of alternative, larger protein nanopores such as cytolysin A from *Salmonella typhi* (ClyA),¹⁹ ligand binding and enzyme conformational dynamics have been observed at the single-molecule level.^{20, 21} Such techniques have been termed “nanopore enzymology”.²² As for the many groundbreaking single-molecule enzymology studies that have used fluorescence detection,^{23, 24} nanopore enzymology has the potential to elucidate features not accessible using ensemble methods, with the distinct benefit of being label-free. Conformational motions and individual mechanistic steps, for example, can be resolved that would be hidden in ensemble measurements if they were not rate determining steps. Single-molecule techniques can reveal heterogeneity and disorder in reactions that would similarly disappear in an ensemble average.²⁵ Previously, we were also able to measure very high association rate constants that

would be difficult to determine with surface plasmon resonance, another label-free approach, due to limitations in mass transfer at the surface of the sensor chip.²⁶

We have previously developed engineered protein nanopores (**Figure 1a**) for the detection and analysis of the PIM family of protein kinases,²⁶ and further applied the technology to develop a label-free screening technique for PIM kinase inhibitors.²⁷ The PIM kinases are a family of three constitutively-active serine/threonine protein kinases implicated in many cancers and leukemia, and are therefore under investigation as therapeutic targets.²⁸ So far, our investigations have focused on the binding of substrate (or pseudosubstrate) and nucleotides/inhibitors, but not the reversible conversion of substrate by phosphorylation and dephosphorylation that is so critical for the signaling pathways underpinning life.

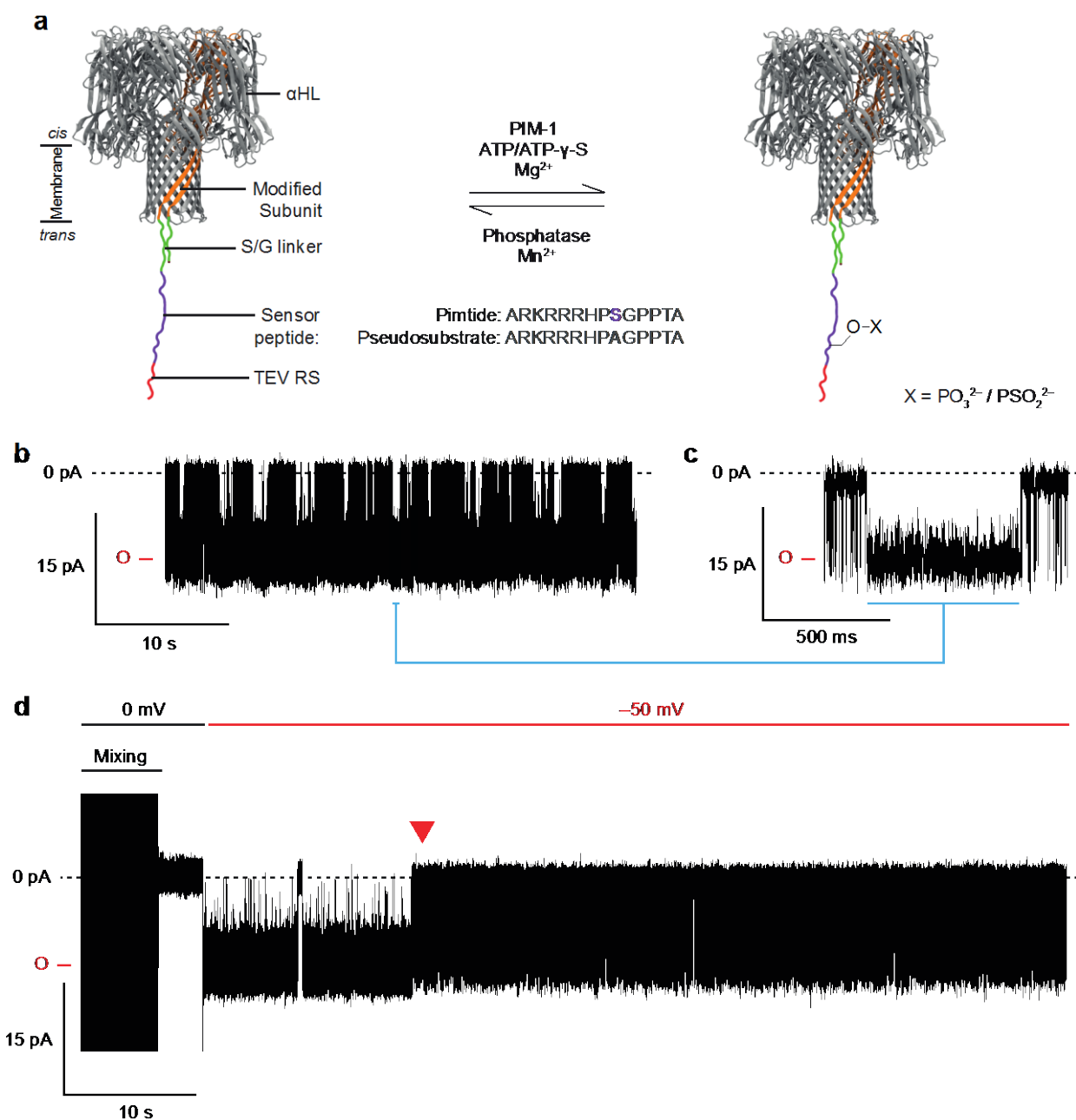


Figure 1. Phosphorylation of α HL-D127N-PLM-TEV. (a) Structural illustration of the sensor pore and reaction scheme for reversible phosphorylation/thiophosphorylation. The sensor peptide (Pimtide/pseudosubstrate) is fused within the beta-turn of one subunit of alpha-hemolysin (α HL). The phosphoacceptor Ser residue of Pimtide is indicated in purple. Site-specific proteolytic cleavage by TEV protease at the incorporated recognition site (TEV RS) liberates one end of the sensor peptide to produce the sensor pore as depicted. (b) Representative current trace of α HL-

D127N-PLM-TEV in the presence of 191 nM PIM-1. A single binding event is highlighted by the blue line and in (c) is shown expanded in the time dimension. Kinase binding appears as prolonged events at the open pore current level. Blockade events arise due to interactions of the sensor peptide with the pore mouth while the enzyme is not bound, as previously reported.²⁶ (d) Representative current trace of phosphorylation occurring in real time on α HL-D127N-PLM-TEV in the presence of 191 nM PIM-1. 1 mM MgCl_2 and 500 μM ATP (final concentrations) were added to the trans compartment, which was mixed with a magnetic stirrer bar for approximately 30 s. After mixing a potential of -50 mV was applied and two binding events were observed immediately preceding phosphorylation (indicated by the red triangle), whereupon binding events were almost entirely abolished thereafter. The measurement buffer was 15 mM MOPS, pH 6.8, 300 mM KCl, 5 mM DTT.

Here we report the observation of protein phosphorylation occurring on a single molecule of substrate. Similarly, using the ATP analogue ATP- γ -S, we were able to observe thiophosphorylation. We were also able to indirectly observe the reverse process of dephosphorylation by a protein phosphatase. Finally, we investigated the role of Mg^{2+} and Mn^{2+} upon substrate and product binding, and uncovered a Mn^{2+} -induced enhancement of a weak synergistic binding effect exhibited by ATP- γ -S. Together with our previous work, we show that the full gamut of protein kinase behavior can be studied with appropriately-designed nanopore experiments, demonstrating the power of nanopore enzymology as a complementary tool to conventional enzymology and other single-molecule techniques.

Results and discussion

Observation of phosphorylation with a nanopore

We began by testing whether we could observe phosphorylation of the α HL-D127N-PLM-TEV pore (**Figure 1a**, where the sensor peptide is the consensus substrate sequence ‘Pimtide’)²⁹ during single-channel electrical measurements. A single pore was inserted into a planar lipid bilayer and PIM-1 was added to a final concentration of 191 nM in the *trans* compartment. Kinase binding was monitored for five minutes (**Figure 1b and c**) before 500 μ M ATP and 1 mM MgCl₂ (final concentrations) were added to the *trans* compartment with mixing. Shortly after the addition of MgATP, the previously observed binding events of the kinase were almost entirely abolished (**Figure 1d and 2b,c**). Although the change in signal almost always occurred during the thirty-second mixing period, and so was obscured by noise associated with the mixing, we were occasionally able to directly observe the change in binding kinetics, where binding events of long duration (seconds) immediately preceded the apparent abolishment of binding (as shown in **Figure 1d**). This change in binding kinetics appeared to be irreversible, as no further changes, or reversion to the previous kinetics, were observed even in long recordings (>1h). We therefore reasoned that the altered binding kinetics were due to phosphorylation of the pore.

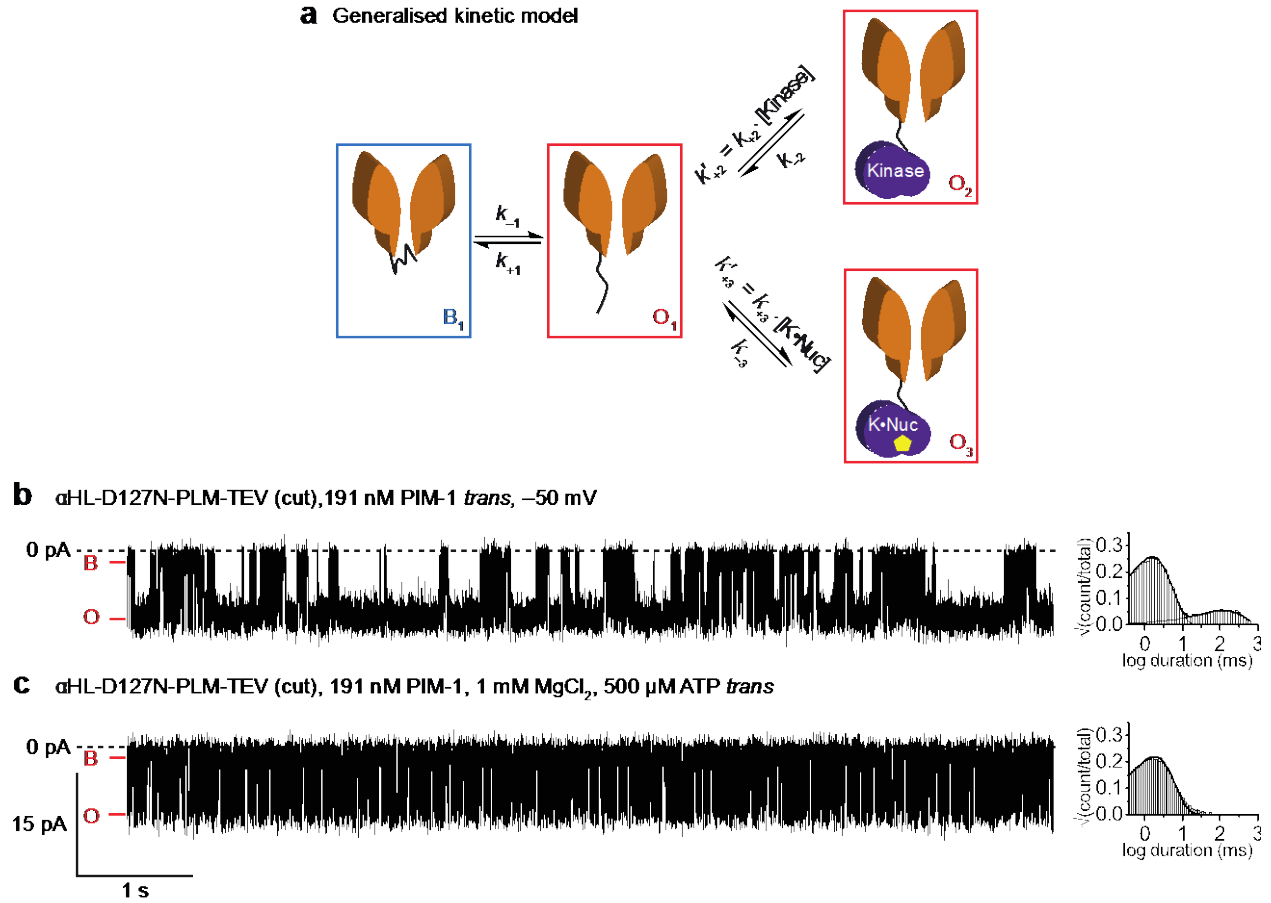


Figure 2. Analysis of phosphorylation. (a) Generalised kinetic model used for analysis of single channel recordings. States O1 and B1 correspond to the open and blocked (by the sensor peptide) current levels of the sensor pore respectively. In the presence of kinase, state O2 corresponds to the open current level with longer event duration caused by binding of the kinase to the sensor pore. In the presence of nucleotides that synergistically bind, state O3 corresponds to the open current level caused by formation of the ternary complex. Binary and ternary complex formation is assumed to be independent, reflecting equilibrium concentrations in solution.²⁷ (b–c) Representative current traces and open-pore current level dwell-time histograms are shown for the α HL-D127N-PLM-TEV pore in the presence of 191 nM PIM-1 (b) before and (c) after the addition of MgATP and subsequent phosphorylation of the sensor peptide. The blocked (B) and open (O) pore current levels are indicated in red, where blockade of the pore arises due to the

dynamics of the sensor peptide.²⁶ States O1, O2 and O3 share the same open pore current level, as previously reported,²⁶ but differ in their mean dwell times.

Kinetic analysis was performed on single-channel recordings taken before and after phosphorylation, as previously described.^{26, 27} Before phosphorylation, the model with states B1, O1 and O2 was used (**Figure 2a**), and binding of PIM-1 was consistent with previous measurements, with $k_{+2} = (1.4 \pm 0.3) \times 10^8 \text{ M}^{-1} \text{ s}^{-1}$, $k_{-2} = 9 \pm 1 \text{ s}^{-1}$, and $K_d = 70 \pm 20 \text{ nM}$ (all $n = 6$, **Figure 2b**). The unusually high association rate constant for this interaction was previously found to be due to electrostatic enhancement.²⁶ The mean interevent interval (corresponding to intervals between sensor peptide blockade events) was $1.2 \pm 0.1 \text{ ms}$ (all $n = 6$) and the mean blockade duration (corresponding to dwell times in the blocked pore current level) was $5 \pm 1 \text{ ms}$. After phosphorylation, the population of kinase binding events was almost entirely abolished (**Figure 2c**). Analysis was therefore performed with a model only containing states B1 and O1 (**Figure 2a**). The mean interevent interval was $1.3 \pm 0.2 \text{ ms}$ and the mean blockade duration of the sensor peptide was $6 \pm 2 \text{ ms}$ (all $n = 6$).

To support our conclusion that we had observed phosphorylation, we also tested whether $\alpha\text{HL-D127N-PLM-TEV}$ was phosphorylated by PIM-1 in bulk. $\alpha\text{HL-D127N-PLM-TEV}$ and $\alpha\text{HL-D127N-PSLM-TEV}$ (pseudosubstrate variant, **Figure 1a**) pores were incubated in phosphorylation reactions spiked with radioactive $\gamma\text{-}^{33}\text{P}\text{-ATP}$ and then analyzed by SDS-PAGE followed by autoradiography and Coomassie staining. A strong band of radioactivity was found coincident with the Coomassie-stained band for $\alpha\text{HL-D127N-PLM-TEV}$, but not for $\alpha\text{HL-D127N-PSLM-TEV}$, and only when kinase was present (**Supplementary Figure 1**). This

confirmed that the substrate-bearing pore was phosphorylated on the serine of the Pimtide substrate, which is mutated to alanine in the pseudo-substrate variant.

Divalent metal ions affect product binding

Many kinases have two divalent metal ion (M^{2+}) coordination sites. The first, essential, metal ion (Me2) is believed to bind as Mg^{2+} -ATP, whereas Me1 is occupied at higher concentrations (mM for Mg^{2+} with the catalytic subunit of cAMP-dependent protein kinase (PKA)) and leads to a reduction in turnover rate.³⁰⁻³⁴ Although Me1 stabilizes the enzyme—substrate complex, it also slows product release.³⁵ We therefore repeated our single-channel phosphorylation experiments at a higher Mg^{2+} concentration (10 mM). Although this experiment does not allow access to turnover rates, we observed a new population of events that we attribute to product binding, which would also have an inhibitory effect on turnover (**Supplementary Figure 2a**). In support of our conclusion that these events are product binding, increased concentration of PIM-1 gave an increased frequency of events (**Supplementary Figure 2b**).

As a final confirmation that we were observing product binding after phosphorylation of the pore, we phosphorylated α HL-D127N-PLM-TEV in bulk solution and then purified the resulting ‘phospho-pore’. When inserted into planar lipid bilayers, these phospho-pores exhibited the same two-state kinetics as unphosphorylated α HL-D127N-PLM-TEV in the absence of kinase, with a mean interevent interval of 1.3 ± 0.2 ms and mean blockade duration of 6.9 ± 0.9 ms (both $n = 6$; **Supplementary Figure 3a**). When PIM-1 was added to a final concentration of 162 nM in the *trans* compartment, the behavior of the pore was unchanged, with a mean interevent interval of 1.5 ± 0.3 ms and mean blockade duration of 8 ± 1 ms (both $n = 5$) (**Supplementary Figure 3b**). Upon the subsequent addition of $MgCl_2$ to a final concentration of 10 mM (the high Mg^{2+} condition, as described above), the innate pore blockades were unchanged, with a mean

interevent interval of 1.4 ± 0.2 ms and mean blockade duration of 8 ± 2 ms (both $n = 4$). Consistent with our previous observations, we saw a new and substantial population of events in the open pore current level with a mean duration of 6 ± 1 ms ($n = 4$, **Supplementary Figure 3c**). The resulting rate constants for this product binding were $k_{+2} = (1.9 \pm 0.5) \times 10^8 \text{ M}^{-1} \text{ s}^{-1}$, $k_{-2} = 170 \pm 40 \text{ s}^{-1}$, giving $K_d = 900 \pm 300 \text{ nM}$ (all $n = 4$).

Finally, we found that the subsequent addition of 1 mM MnCl_2 (final concentration) after 10 mM MgCl_2 altered the kinetics of this product binding. After the addition of MnCl_2 , the mean event duration of product binding increased to 17 ± 4 ms ($n = 5$, **Supplementary Figure 3d**). The mean association rate k_{+2} decreased to $(9 \pm 1) \times 10^7 \text{ M}^{-1} \text{ s}^{-1}$, k_{-2} decreased to $60 \pm 10 \text{ s}^{-1}$, giving $K_d = 700 \pm 200 \text{ nM}$ ($n = 5$).

Thiophosphorylation of the nanopore substrate

Adenosine-5'-(γ -thio)-triphosphate (ATP- γ -S) is used as a kinase substrate to yield thiophosphorylated proteins that are resistant to hydrolysis by protein phosphatases. A thiophosphorylated pore might be useful as a sensor for protein phosphatases, as they would be expected to bind and dissociate repeatedly without hydrolyzing the thiophosphorylated sensor peptide. We therefore investigated thiophosphorylation of the $\alpha\text{HL-PLM-TEV}$ pore.

Before addition of $\text{MgATP-}\gamma\text{-S}$, PIM-1 bound with rate constants $k_{+2} = (1.7 \pm 0.2) \times 10^8 \text{ M}^{-1} \text{ s}^{-1}$, $k_{-2} = 8 \pm 1 \text{ s}^{-1}$, giving $K_d = 44 \pm 7 \text{ nM}$ ($n = 4$). The mean interevent interval of the innate pore blockade from the sensor peptide was 1.6 ± 0.3 ms and the mean blockade duration was 8 ± 1 ms ($n = 4$, **Supplementary Figure 4a**). After addition of $\text{MgATP-}\gamma\text{-S}$, events due to kinase binding appeared to be almost entirely abolished (**Supplementary Figure 4b**). The mean interevent interval of the innate pore blockade from the sensor peptide was 1.3 ± 0.2 ms and the mean blockade duration was 15 ± 2 ms ($n = 4$). The mean blockade duration of the thiophosphorylated

sensor peptide was therefore approximately twice as long than that for the peptide in the phosphorylated or unphosphorylated states.

We then investigated whether we could observe phosphatase binding to the thiophosphorylated sensor pore. Lambda protein phosphatase (LamPP) is a Mn^{2+} -dependent protein phosphatase that releases phosphate from phosphorylated serine, threonine and tyrosine residues.^{36, 37} Although not mammalian, it shares some similarities to the catalytic subunits of PP1, PP2A and PP2B groups in humans, and is readily obtained, either commercially or by expression in *E. coli*.

After thiophosphorylation, the presence of 1 mM MnCl_2 appeared to enhance product binding in a similar manner to that seen with the phosphorylated pore (**Supplementary Figure 5a,b**). A population of binding events was discernible with mean duration of 21 ± 6 ms ($n = 4$, **Supplementary Figure 5b**). Kinetic analysis yielded a mean association rate constant of $(6 \pm 2) \times 10^7 \text{ M}^{-1} \text{ s}^{-1}$ and mean dissociation rate constant of $50 \pm 10 \text{ s}^{-1}$, giving $K_d = 800 \pm 300 \text{ nM}$ (all $n = 4$). Subsequent addition of 20–400 nM LamPP (final concentration) produced no discernible alteration in pore behavior (**Supplementary Figure 5c**). Possible reasons for not being able to detect LamPP binding may be the smaller size of LamPP or fast binding kinetics not resolvable within the time resolution of our experiment.

Phosphorylated nanopore turnover by a protein phosphatase

As we were able to observe behavior consistent with phosphorylation of a single pore reconstituted into a lipid bilayer, we were curious whether we could also observe the opposing process—dephosphorylation of an already phosphorylated pore by a protein phosphatase. We reconstituted purified phospho-pore (as described above) into lipid bilayers. First, 1 mM MnCl_2 was added and the pore was observed for five minutes (**Figure 3a (i)**), after which 400 nM LamPP was added (both final concentrations). We did not observe any change in the electrical

behavior of the pore over 45 minutes after LamPP addition (**Figure 3a (ii)**). The sensor peptide blocking kinetics of phosphorylated α HL-D127N-PLM-TEV are indistinguishable from those of the unphosphorylated pore, so it was not possible to use these to infer a change in the phosphorylation state of the pore after the addition of LamPP and MnCl_2 . As with our previous observations of the thiophosphorylated pore with LamPP, binding of LamPP to the sensor peptide appears not to be detectable, perhaps due to very short residence times or the smaller size of LamPP compared with the Pim kinases. Further, dephosphorylation may simply occur too rapidly for LamPP binding to be observed.

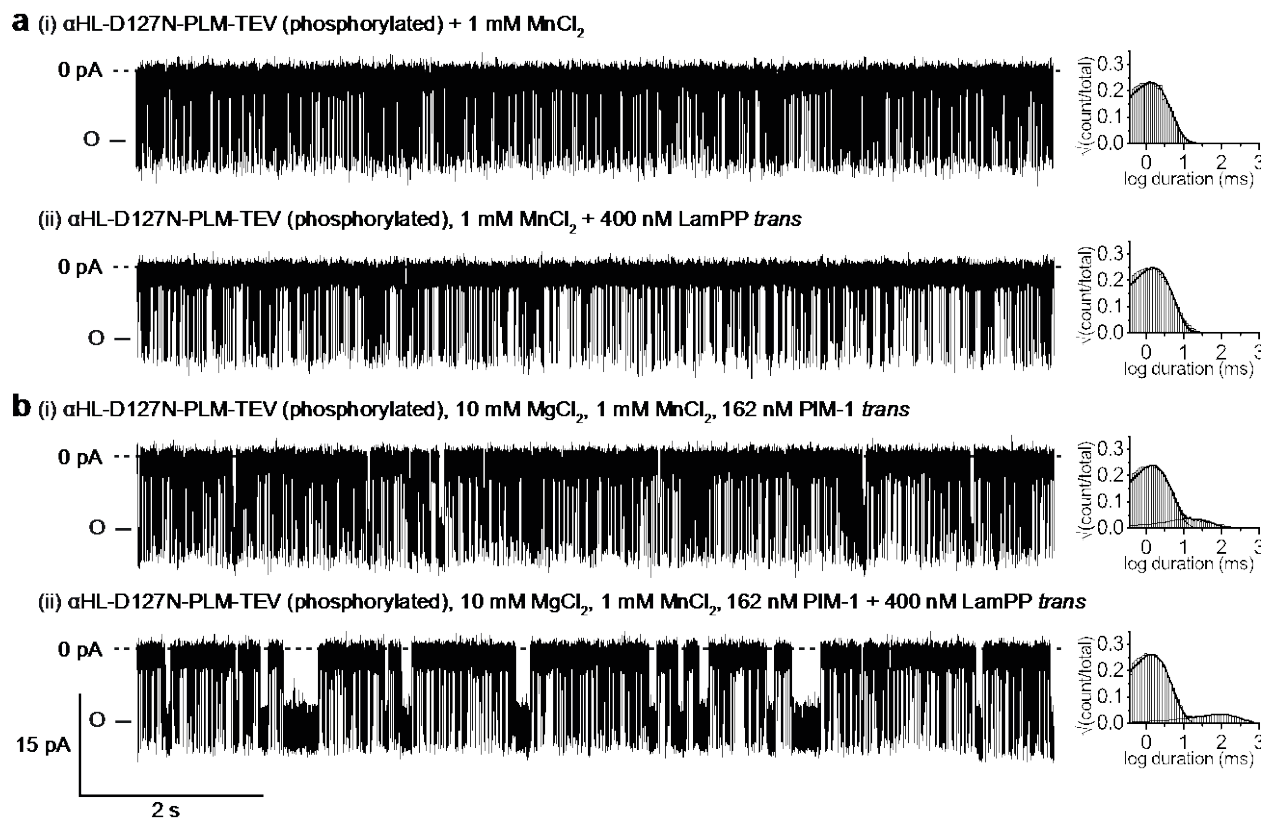


Figure 3. Dephosphorylation of phosphorylated α HL-D127N-PLM-TEV by lambda protein phosphatase. Phosphorylated and purified α HL-D127N-PLM-TEV was reconstituted into lipid bilayers and measured under an applied potential of -50 mV. (a) Representative current traces

and open-pore current level dwell-time histograms are shown for the pore in the presence of 1 mM MnCl_2 , (i) before and (ii) 30 minutes after the addition of 400 nM LamPP (final concentration) to the *trans* compartment. (b) Representative traces and histograms are shown for phosphorylated $\alpha\text{HL-D127N-PLM-TEV}$ in the presence of 10 mM MgCl_2 , 1 mM MnCl_2 , and 162 nM PIM-1 (i) before and (ii) after the addition of 400 nM LamPP (final concentration) to the *trans* compartment. The trace and histogram for (b)(ii) were obtained after addition of LamPP and mixing of the *trans* compartment for 30 seconds. The open-pore current level is marked 'O'. Measurements were performed in 15 mM MOPS, pH 6.8, 300 mM KCl, 5 mM DTT. The filter corner frequency was 2 kHz.

As PIM-1 has markedly different binding kinetics for the unphosphorylated and phosphorylated forms of $\alpha\text{HL-D127N-PLM-TEV}$, we tested whether it could be used as a reporter of the phosphorylation state of the sensor peptide. In this way, we hoped to confirm if LamPP could indeed bind and dephosphorylate the phospho-pore. We began by reconstituting a phosphorylated $\alpha\text{HL-D127N-PLM-TEV}$ pore into a lipid bilayer, followed by the addition of PIM-1 to a final concentration of 162 nM in the *trans* compartment. After observing the pore for five minutes, 10 mM MgCl_2 and 1 mM MnCl_2 (final concentrations) were each added in turn to the *trans* compartment and kinase binding was further observed for around five minutes after each addition, as reported above (**Figure 3b (i)**). Upon the subsequent addition of 400 nM LamPP (final concentration), PIM-1 binding consistent with that observed with an unphosphorylated pore was rapidly initiated (**Figure 3b (ii)**). This change of binding kinetics always occurred within the time taken to mix the contents of the *trans* compartment (approximately 30 seconds). The mean event duration of PIM-1 binding increased from

17 ± 4 ms to 80 ± 10 ms ($n = 3$), and the mean association rate constant decreased slightly, with $k_{+2} = (9 \pm 1) \times 10^7 \text{ M}^{-1} \text{ s}^{-1}$ before LamPP and $k_{+2} = (6.3 \pm 0.8) \times 10^7 \text{ M}^{-1} \text{ s}^{-1}$ after (both $n = 3$). The innate blockade events of the pore were unchanged. We conclude that LamPP is able to dephosphorylate the phospho-pore, but its binding is not directly observable under the experimental conditions.

We also attempted the addition of ATP (10 μM final concentration) after the dephosphorylation step described in the preceding paragraph, to see if we could reconstitute a full phosphorylation—dephosphorylation cycle. We saw new events in the open current level with a mean duration of the order of 1 s. However, this population was sparse (even after 20–30 min recording) and the event dwell time histogram could not be satisfactorily fitted. In our previous studies, we found PIM-1 to have a very high association rate constant ($\sim 10^8 \text{ M}^{-1} \text{ s}^{-1}$). Further, k_{cat} is around 4 s^{-1} ,³⁸ whereas the dissociation rate constant of the ternary complex (measured using the pseudosubstrate sensor)²⁷ is $\sim 0.09 \text{ s}^{-1}$, suggesting that formation of a productive ternary complex virtually always leads to phosphorylation and hence fast product dissociation. It is therefore possible that under our conditions the sensor peptide is rarely in the unphosphorylated state long enough to be observed, due to the efficiency of PIM-1.

Mn²⁺ relaxes nucleotide selectivity

We have previously used a pseudosubstrate-variant of $\alpha\text{HL-D127N-PLM-TEV}$, called $\alpha\text{HL-D127N-PSLM-TEV}$, to investigate binding synergism between the pseudosubstrate and MgATP without subsequent reaction of the substrate.²⁷ As we showed above that ATP- γ -S could be used by PIM-1 to thiophosphorylate the substrate-bearing pore, we further investigated the interaction of this ATP analogue with the pseudosubstrate pore variant.

With 10 μM ATP- γ -S in the presence of 162 nM PIM-1 and 10 mM MgCl_2 , no additional population of binding events was observed (**Supplementary Figure 6a,b**). The kinetics of PIM-1 were altered from $k_{+2} = (1.4 \pm 0.1) \times 10^8 \text{ M}^{-1} \text{ s}^{-1}$ and $k_{-2} = 10 \pm 1 \text{ s}^{-1}$, to $k_{+2} = (8.6 \pm 0.5) \times 10^7 \text{ M}^{-1} \text{ s}^{-1}$ and $k_{-2} = 17 \pm 1 \text{ s}^{-1}$ (all $n = 3$), which is entirely attributable to the effect of MgCl_2 , as previously identified.²⁷ At 100 μM ATP- γ -S a small population of events with a longer dwell time than those corresponding to the binary complex with PIM-1 were observed (**Supplementary Figure 6c**), reminiscent of those seen with MgATP.²⁷ This suggested synergistic binding of MgATP- γ -S, but considerably weaker than that of MgATP.

We also tested these conditions with the further addition of 1 mM MnCl_2 (final concentration) and found a dramatic enhancement of this synergistic effect. With 10 μM ATP- γ -S, events of long duration that were previously not observed with only Mg^{2+} were now prominent and formed a substantial population after the addition of Mn^{2+} (**Supplementary Figure 6d**). At 100 μM ATP- γ -S, the ternary population dominated, with events corresponding to the binary complex becoming sparse, necessitating the k_{-2} rate constant to be fixed to the average value obtained at the lower ATP- γ -S concentration (**Supplementary Figure 6e**). Traces were analyzed with the same kinetic model used for the MgATP synergistic effect²⁷ (**Figure 2a**), and the resulting rate constants are summarized in **Table 1** (all $n = 3$).

In the case of PKA, synergistic binding of ATP is approximately 100-fold stronger than for ADP or AMP-PNP.³⁹ Thus, there appear to be quite specific conformational requirements around the terminal phosphate for strong synergistic binding, which the γ -thio substitution presumably disrupts in the case of ATP- γ -S with PIM-1, and which Mn^{2+} appears to restore, relaxing nucleotide specificity.

Conclusion

In summary, we have observed phosphorylation, thiophosphorylation, and dephosphorylation occurring on a single substrate molecule using our nanopore sensor. Together with our previous work, this demonstrates the versatility and power of the nanopore enzymology approach. Further, we have characterized the effect of divalent metal ion coordination upon key mechanistic steps, such as product binding.

We found that product binding is M^{2+} -dependent, with higher concentrations enhancing product binding, presumably *via* occupation of the Me1 site. Further, this effect appears to be stronger for Mn^{2+} over Mg^{2+} . In the case of PKA, divalent metal ions other than Mg^{2+} were found to stabilize both the enzyme substrate and product complexes, largely in line with the Irving-Williams series.⁴⁰ Further, conformational changes in PKA are important for key steps in the mechanism such as product release.⁴¹⁻⁴³ For PIM-1, the association rate constant for binding of the phospho-peptide is largely unchanged *versus* the substrate peptide, whereas the phospho-peptide dissociates more rapidly once bound. We therefore propose that the phospho-peptide is bound in a less stable, ‘open’ conformation of the kinase, resulting in its lower affinity. For PKA under high Mg^{2+} conditions (10 mM), the rate-determining step is release of ADP, and this appears to require loss of the Mg^{2+} ion at Me1.^{30, 34, 41} In our experiments with PIM-1 we see that high Mg^{2+} and, more strongly, Mn^{2+} delays release of the bound phospho-peptide, which suggests that coordination stabilizes a more tightly bound, ‘closed’ kinase conformation. Interestingly, this appears to also be the case in the absence of nucleotide.

Further, we found that Mn^{2+} relaxes nucleotide specificity, as demonstrated by the enhanced synergistic binding between the ATP analogue ATP- γ -S and pseudo-substrate sensor pore. Key rate constants and dissociation constants are summarized in **Table 1**. Indeed, it was observed for PKA that ternary complex formation with an inhibitory peptide in the presence of Mg^{2+} was

highly specific to ATP, whereas Mn^{2+} appeared to relax this specificity, allowing the formation of complexes with ITP, GTP and AMP-PNP.⁴⁴ Further, Mn^{2+} appears to enhance the binding of ADP to PKA.^{32, 40, 45} Our findings therefore support the conclusion that reduced turnover in the presence of Mn^{2+} likely arises due to delayed product release of both ADP and peptide. While the Mn^{2+} concentration used here is higher than normal physiological conditions, concentrations can be elevated due to disease. Further, the implications of the combined effects of Mn^{2+} observed here may be important for the interpretation of structural studies, where it is common to crystallize protein kinases in the presence of Mn^{2+} .

Table 1. Association and dissociation rate constants and equilibrium dissociation constants for PIM-1 binding to sensor pores

Sensor pore	[Mg ²⁺] / mM	[Mn ²⁺] / mM	<i>k</i> ₊₂ / 10 ⁸ M ^{−1} s ^{−1} [a]	<i>k</i> _{−2} / s ^{−1} [b]			<i>K</i> _d / nM
αHL-D127N-PLM-TEV	0	0	1.4 ± 0.3	9 ± 1			70 ± 20
Phosphorylated ^[c]	10	0	1.9 ± 0.5	170 ± 40			900 ± 300
	10	1	0.9 ± 0.1	60 ± 10			700 ± 200
Thiophosphorylated ^[d]	10	1	0.6 ± 0.2	50 ± 10			800 ± 300
αHL-D127N-PSLM-TEV	[ATP-γ-S] / μM			<i>k</i> _{−3} / s ^{−1} [e]			
	10	0	10	0.86 ± 0.05	17 ± 1	negligible	200 ± 20
	10	0	100	N.D.	12 ± 3	0.8 ± 0.4	N.D.
	10	1	10	N.D.	43 ± 7	1.0 ± 0.2	N.D.
	10	1	100	N.D.	43.2 ^[f]	0.52 ± 0.03	N.D.

N.D. = Not determined, PLM = Pimtide Loop Mutant, PSLM = Pseudosubstrate Loop Mutant. [a] Association rate constant for binary complex formation. [b] Dissociation rate constant for the binary complex. [c] Measured in absence of ATP; product binding was negligible for $[\text{Mg}^{2+}] = 1 \text{ mM}$. [d] In the presence of $100 \mu\text{M ATP-}\gamma\text{-S}$; product binding was negligible in the absence of Mn^{2+} . [e] Dissociation rate constant for the ternary complex. [f] Fixed fitting parameter.

Our observations will form the basis for further studies aimed at full conformational resolution of the catalytic cycle of protein kinases. A limitation of our current sensor is that the kinase is

bound some distance from the pore and detected through modulation of the substrate peptide's gating of the pore. Further, the phosphorylated pore is only indirectly distinguishable from its unmodified state (although interestingly the thiophosphorylated pore does exhibit an altered signal), and phosphatase binding is detected indirectly. Nonetheless, the ability to observe the enzymatic conversion of a single substrate molecule is an advance over previous nanopore methods that have relied on the detection of reaction products translocating the pore from bulk solution, as such strategies lose many of the benefits of true single molecule measurements. As previously discussed,²⁶ our proteolytically cleaved sensor peptide strategy (**Figure 1b**) is designed to relax the conformational constraints arising from fusion of a β -hairpin loop at the pore mouth. However, the conformational constraints within full-size substrates may still vary from those of our nanopore sensors bearing short peptides. Nonetheless, the parameters that we have measured so far are in good agreement with counterparts in the literature derived by using other techniques.

To enhance the capabilities of our method further, we envisage enhanced nanopore sensors derived from alternative protein pores (for example CsgG, MspA, aerolysin, FhuA or FraC). In particular, the use of larger pores such as ClyA (**Figure 4**)¹⁹ may prove beneficial. Detection within the lumen of such pores will enable greater sensitivity to binding species, phosphorylation states, and even allow us to observe conformational changes in the enzyme during catalysis. Nanopore enzymology therefore has the potential to gain exquisite mechanistic insight, free from labels and at the single-molecule level.

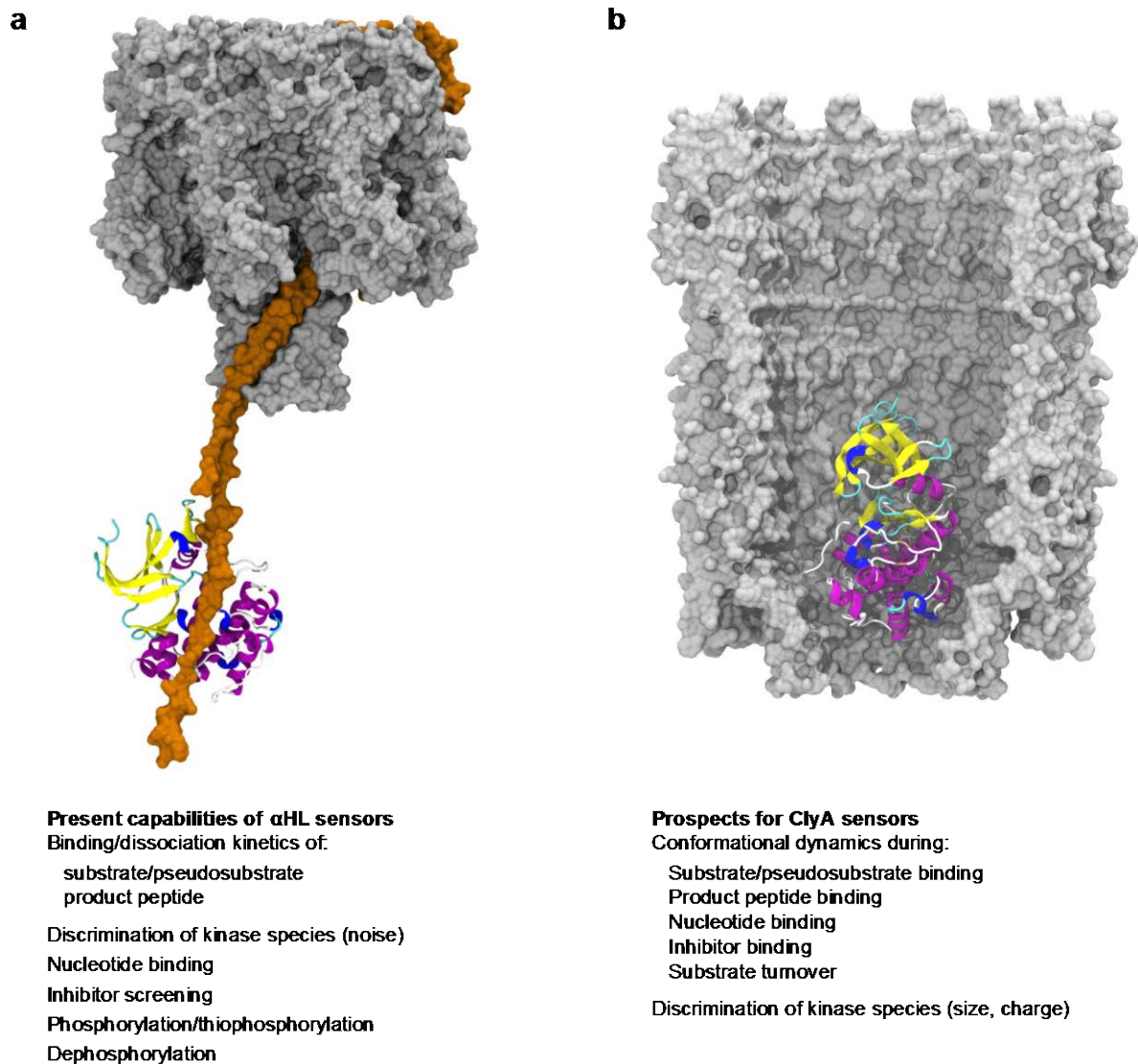


Figure 4. Future prospects in kinase sensing. Scale renderings of (a) the α HL-derived Pim kinase sensor with PIM-1 bound; (b) a proposed sensor derived from cytolysin A (ClyA) with PIM-1 within the pore lumen (pore shown in cutaway). Atomic coordinates were derived from PDB structures: 7AHL (α HL), 2BIL (PIM-1), 2WCD (ClyA).

Materials and Methods

Unless otherwise indicated, chemicals and oligonucleotides were purchased from Sigma Aldrich (Merck).

α HL pores

α HL-D127N-PLM-TEV and α HL-D127N-PSLM-TEV pores were prepared as previously described.^{26, 27}

Nucleotides

ATP stock solutions were prepared from the ATP disodium salt hydrate and titrated to pH 6.9 with 1 M Tris base. ATP concentration was confirmed spectrophotometrically at 259 nm using an extinction coefficient of 15,400 M⁻¹ cm⁻¹. Stocks were stored at –80°C as single-use aliquots.

Adenosine-5'-(γ -thio)-triphosphate (ATP- γ -S) was purchased as the tetralithium salt from Tocris Bioscience. Stock solutions were prepared in the same manner as for ATP.

γ -[³³P]-ATP (3000 Ci mmol⁻¹, 10 mCi ml⁻¹) was purchased from Perkin Elmer.

Enzymes

PIM-1 was expressed, purified and quantitated as previously described.^{26, 46} Lambda protein phosphatase was purchased from New England Biolabs.

In vitro phosphorylation reactions

α HL monomers (α HL-D127N, α HL-D127N-PLM-TEV-D8, α HL-D127N-PSLM-TEV-D8) without L-[³⁵S]-methionine labelling were prepared by *in vitro* transcription and translation (IVTT) as previously described,^{26, 27} but with L-[³⁵S]-Met omitted from the reaction mixture. TEV protease cleavage and oligomerization to produce heteromers was performed as previously.²⁶ Radioactively labelled equivalents were also produced and electrophoresed in lanes adjacent to those of the unlabeled proteins. These served as markers to allow the locations of the

unlabeled proteins to be inferred and the bands accurately excised and extracted from the gel, as previously described.

Phosphorylation reactions were performed in 15 mM MOPS pH 6.8, 300 mM KCl, 5 mM DTT, 1 mM MgCl₂ and 0.1% Tween-20. 100 µl of purified αHL heteroheptamer (~1 ng µl⁻¹) was used per reaction as substrate. Each protein sample was concentrated to a final volume of 20 µl and simultaneously the buffer was exchanged with the phosphorylation reaction buffer by repeated cycles of concentration and dilution in Microcon YM-50 centrifugal filters (50 kDa molecular weight cut-off, Millipore). PIM-1 was added to a final concentration of 200 nM, and reactions were initiated by adding 50 µM (final concentration) of ATP spiked with 10 µCi γ-[³³P]-ATP. Reactions were incubated at 30°C for one hour and then stopped by the addition of 5 µl 5X Laemmli Sample Buffer [1X=62.5 mM Tris.HCl pH6.8, 2.3% (w/v) SDS, 5% (v/v) β-mercaptoethanol, 10% (w/v) glycerol]. Samples were then electrophoresed in a 5% SDS-PAGE gel. The gel was stained with Coomassie blue (Instant Blue, Expedeon) before being dried on Whatman 3M filter paper under vacuum for 1.5 h at 75°C. The gel was then autoradiographed using Kodak BioMax MR film. The protein standards were Precision Plus dual color protein standards (Bio-Rad); the radioactive protein standards were [Methyl-¹⁴C] methylated protein molecular weight markers (1 µCi, Perkin Elmer).

Preparation of phosphorylated αHL-PLM-TEV heteromers

To prepare αHL-PLM-TEV heteromers phosphorylated in bulk, αHL-D127N-PLM-TEV-D8 was produced by IVTT with L-[³⁵S]-methionine labelling, as previously described.²⁶ After the IVTT reaction had proceeded for 1 h, it was stopped by the addition of 34 µg ml⁻¹ chloramphenicol. 200 nM PIM-1, 1 mM MgCl₂, 50 µM ATP, and 10 U AcTEV protease (Invitrogen) were added to the stopped reaction mixture, which was then incubated at 4°C for

4 h. Heteromer formation and purification by SDS-PAGE, and gel extraction were then performed as previously described.²⁶

Single-channel recording and current analysis

Single-channel recording was performed using the Montal-Mueller method as previously described.²⁶ The *trans* compartment was mixed after the addition of enzymes and other reagents for 30 s. This was achieved using a magnetic stirring flea (Sigma Aldrich) operated from underneath the electrophysiology chamber by a rotating bar magnet. Current recordings were idealized and rate constants estimated using QuB 2.0 (www.qub.buffalo.edu) as previously described.²⁶ Data were plotted and fitted in OriginPro 9 (OriginLab). Fitting was performed without error weighting. Data are reported as mean \pm s.d. unless otherwise indicated.

ASSOCIATED CONTENT

The authors declare the following competing financial interest: Hagan Bayley is the Founder of, a consultant for, and a share-holder of Oxford Nanopore Technologies, a company engaged in the development of nanopore sensing and sequencing technologies.

Supporting Information.

The following files are available free of charge.

Supplementary Figures 1–6 (PDF)

AUTHOR INFORMATION

Corresponding Authors

*Email: harrington@biochem.mpg.de or hagan.bayley@chem.ox.ac.uk

Present Addresses

† Max Planck Institute of Biochemistry, Am Klopferspitz 18, 82152 Martinsried, Germany

‡ SIB Swiss Institute of Bioinformatics, Personalized Health Informatics, CH-4056 Basel, Switzerland

§ Institute for Pharmaceutical Chemistry, Structural Genomics Consortium and Buchmann Institute for Molecular Life Sciences, Johann Wolfgang Goethe-University, Frankfurt am Main, Germany

Author Contributions

L.H. and H.B. designed experiments. L.H. performed all experiments and wrote the manuscript. L.T.A and S.K. supplied key reagents and advice. All authors reviewed and revised the manuscript.

ACKNOWLEDGMENTS

This work was supported by grants from the National Institutes of Health and Oxford Nanopore Technologies. L.H. was supported in part by a Biotechnology and Biological Sciences Research Council doctoral training grant. S.K. and L.T.A. are supported by the Structural Genomics Consortium, a registered charity (number 1097737) that receives funds from AbbVie, Bayer Pharma AG, Boehringer Ingelheim, Canada Foundation for Innovation, Eshelman Institute for Innovation, Genome Canada, Innovative Medicines Initiative (EU/EFPIA) [ULTRA-DD grant no. 115766], Janssen, Merck KGaA Darmstadt Germany, MSD, Novartis Pharma AG, Ontario Ministry of Economic Development and Innovation, Pfizer, São Paulo Research Foundation-FAPESP, Takeda, and Wellcome [106169/ZZ14/Z].

REFERENCES

1. Bayley, H.; Cremer, P. S., Stochastic Sensors Inspired by Biology. *Nature* **2001**, *413*, 226-230.
2. Shi, W.; Friedman, A. K.; Baker, L. A., Nanopore Sensing. *Anal Chem* **2017**, *89*, 157-188.
3. Deamer, D.; Akeson, M.; Branton, D., Three Decades of Nanopore Sequencing. *Nat Biotechnol* **2016**, *34*, 518-524.
4. Jain, M.; Olsen, H. E.; Paten, B.; Akeson, M., The Oxford Nanopore Minion: Delivery of Nanopore Sequencing to the Genomics Community. *Genome Biol* **2016**, *17*, 239.
5. Garalde, D. R.; Snell, E. A.; Jachimowicz, D.; Sipos, B.; Lloyd, J. H.; Bruce, M.; Pantic, N.; Admassu, T.; James, P.; Warland, A.; Jordan, M.; Ciccone, J.; Serra, S.; Keenan, J.; Martin, S.; McNeill, L.; Wallace, E. J.; Jayasinghe, L.; Wright, C.; Blasco, J.; Young, S.; Brocklebank, D.; Juul, S.; Clarke, J.; Heron, A. J.; Turner, D. J., Highly Parallel Direct Rna Sequencing on an Array of Nanopores. *Nat Methods* **2018**, *15*, 201-206.
6. Nivala, J.; Marks, D. B.; Akeson, M., Unfoldase-Mediated Protein Translocation through an A-Hemolysin Nanopore. *Nat Biotechnol* **2013**, *31*, 247-250.
7. Rodriguez-Larrea, D.; Bayley, H., Multistep Protein Unfolding During Nanopore Translocation. *Nat Nanotechnol* **2013**, *8*, 288-295.
8. Rosen, C. B.; Rodriguez-Larrea, D.; Bayley, H., Single-Molecule Site-Specific Detection of Protein Phosphorylation with a Nanopore. *Nat Biotechnol* **2014**, *32*, 179-181.
9. Wloka, C.; Van Meervelt, V.; van Gelder, D.; Danda, N.; Jager, N.; Williams, C. P.; Maglia, G., Label-Free and Real-Time Detection of Protein Ubiquitination with a Biological Nanopore. *ACS Nano* **2017**, *11*, 4387-4394.
10. Kukwikila, M.; Howorka, S., Electrically Sensing Protease Activity with Nanopores. *J Phys Condens Matter* **2010**, *22*, 454103.
11. Wang, Y.; Montana, V.; Grubišić, V.; Stout, J., Randy F; Parpura, V.; Gu, L.-Q., Nanopore Sensing of Botulinum Toxin Type B by Discriminating an Enzymatically Cleaved Peptide from a Synaptic Protein Synaptobrevin 2 Derivative. *ACS Appl Mater Interfaces* **2015**, *7*, 184-192.
12. Zhou, S.; Wang, L.; Chen, X.; Guan, X., Label-Free Nanopore Single-Molecule Measurement of Trypsin Activity. *ACS Sens* **2016**, *1*, 607-613.
13. Zhao, Q.; de Zoysa, R. S.; Wang, D.; Jayawardhana, D. A.; Guan, X., Real-Time Monitoring of Peptide Cleavage Using a Nanopore Probe. *J Am Chem Soc* **2009**, *131*, 6324-6325.
14. Mohammad, M. M.; Iyer, R.; Howard, K. R.; McPike, M. P.; Borer, P. N.; Movileanu, L., Engineering a Rigid Protein Tunnel for Biomolecular Detection. *J Am Chem Soc* **2012**, *134*, 9521-9531.
15. Lieberman, K. R.; Cherf, G. M.; Doody, M. J.; Olasagasti, F.; Kolodji, Y.; Akeson, M., Processive Replication of Single DNA Molecules in a Nanopore Catalyzed by Phi29 DNA Polymerase. *J Am Chem Soc* **2010**, *132*, 17961-17972.
16. Olasagasti, F.; Lieberman, K. R.; Benner, S.; Cherf, G. M.; Dahl, J. M.; Deamer, D. W.; Akeson, M., Replication of Individual DNA Molecules under Electronic Control Using a Protein Nanopore. *Nat Nanotechnol* **2010**, *5*, 798-806.

17. Dekker, C., Solid-State Nanopores. *Nat Nanotechnol* **2007**, *2*, 209-215.
18. Howorka, S., Building Membrane Nanopores. *Nat Nanotechnol* **2017**, *12*, 619-630.
19. Soskine, M.; Biesemans, A.; Moeyaert, B.; Cheley, S.; Bayley, H.; Maglia, G., An Engineered Clya Nanopore Detects Folded Target Proteins by Selective External Association and Pore Entry. *Nano Lett* **2012**, *12*, 4895-4900.
20. Soskine, M.; Biesemans, A.; Maglia, G., Single-Molecule Analyte Recognition with Clya Nanopores Equipped with Internal Protein Adaptors. *J Am Chem Soc* **2015**, *137*, 5793-5797.
21. Van Meervelt, V.; Soskine, M.; Singh, S.; Schuurman-Wolters, G. K.; Wijma, H. J.; Poolman, B.; Maglia, G., Real-Time Conformational Changes and Controlled Orientation of Native Proteins inside a Protein Nanoreactor. *J Am Chem Soc* **2017**, *139*, 18640-18646.
22. Willems, K.; Van Meervelt, V.; Wloka, C.; Maglia, G., Single-Molecule Nanopore Enzymology. *Philos Trans R Soc Lond B Biol Sci* **2017**, 372.
23. Lu, H. P.; Xun, L.; Xie, X. S., Single-Molecule Enzymatic Dynamics. *Science* **1998**, *282*, 1877-1882.
24. English, B. P.; Min, W.; van Oijen, A. M.; Lee, K. T.; Luo, G.; Sun, H.; Cherayil, B. J.; Kou, S. C.; Xie, X. S., Ever-Fluctuating Single Enzyme Molecules: Michaelis-Menten Equation Revisited. *Nat Chem Biol* **2006**, *2*, 87-94.
25. Xie, X. S.; Lu, H. P., Single-Molecule Enzymology. *J Biol Chem* **1999**, *274*, 15967-15970.
26. Harrington, L.; Cheley, S.; Alexander, L. T.; Knapp, S.; Bayley, H., Stochastic Detection of Pim Protein Kinases Reveals Electrostatically Enhanced Association of a Peptide Substrate. *Proc Natl Acad Sci U S A* **2013**, *110*, E4417-4426.
27. Harrington, L.; Alexander, L. T.; Knapp, S.; Bayley, H., Pim Kinase Inhibitors Evaluated with a Single-Molecule Engineered Nanopore Sensor. *Angew Chem Int Ed Engl* **2015**, *54*, 8154-8159.
28. Blanco-Aparicio, C.; Carnero, A., Pim Kinases in Cancer: Diagnostic, Prognostic and Treatment Opportunities. *Biochem Pharmacol* **2013**, *85*, 629-643.
29. Hutti, J. E.; Jarrell, E. T.; Chang, J. D.; Abbott, D. W.; Storz, P.; Toker, A.; Cantley, L. C.; Turk, B. E., A Rapid Method for Determining Protein Kinase Phosphorylation Specificity. *Nat Methods* **2004**, *1*, 27-29.
30. Adams, J. A., Kinetic and Catalytic Mechanisms of Protein Kinases. *Chem Rev* **2001**, *101*, 2271-2290.
31. Bao, Z. Q.; Jacobsen, D. M.; Young, M. A., Briefly Bound to Activate: Transient Binding of a Second Catalytic Magnesium Activates the Structure and Dynamics of Cdk2 Kinase for Catalysis. *Structure* **2011**, *19*, 675-690.
32. Herberg, F. W.; Doyle, M. L.; Cox, S.; Taylor, S. S., Dissection of the Nucleotide and Metal-Phosphate Binding Sites in Camp-Dependent Protein Kinase. *Biochemistry* **1999**, *38*, 6352-6360.
33. Zimmermann, B.; Schweinsberg, S.; Drewianka, S.; Herberg, F. W., Effect of Metal Ions on High-Affinity Binding of Pseudosubstrate Inhibitors to Pka. *Biochem J* **2008**, *413*, 93-101.
34. Bastidas, A. C.; Wu, J.; Taylor, S. S., Molecular Features of Product Release for the Pka Catalytic Cycle. *Biochemistry* **2015**, *54*, 2-10.
35. Jacobsen, D. M.; Bao, Z.-Q.; O'Brien, P.; Brooks, r., Charles L.; Young, M. A., Price to Be Paid for Two-Metal Catalysis: Magnesium Ions That Accelerate Chemistry Unavoidably Limit Product Release from a Protein Kinase. *J Am Chem Soc* **2012**, *134*, 15357-15370.

36. Barik, S., Expression and Biochemical Properties of a Protein Serine/Threonine Phosphatase Encoded by Bacteriophage Lambda. *Proc Natl Acad Sci U S A* **1993**, *90*, 10633-10637.
37. Zhuo, S.; Clemens, J. C.; Hakes, D. J.; Barford, D.; Dixon, J. E., Expression, Purification, Crystallization, and Biochemical Characterization of a Recombinant Protein Phosphatase. *J Biol Chem* **1993**, *268*, 17754-17761.
38. Jacobs, M. D.; Black, J.; Futer, O.; Swenson, L.; Hare, B.; Fleming, M.; Saxena, K., Pim-1 Ligand-Bound Structures Reveal the Mechanism of Serine/Threonine Kinase Inhibition by Ly294002. *J Biol Chem* **2005**, *280*, 13728-13734.
39. Lew, J.; Coruh, N.; Tsigelny, I.; Garrod, S.; Taylor, S. S., Synergistic Binding of Nucleotides and Inhibitors to Camp-Dependent Protein Kinase Examined by Acrylodan Fluorescence Spectroscopy. *J Biol Chem* **1997**, *272*, 1507-1513.
40. Knape, M. J.; Ballez, M.; Burghardt, N. C.; Zimmermann, B.; Bertinetti, D.; Kornev, A. P.; Herberg, F. W., Divalent Metal Ions Control Activity and Inhibition of Protein Kinases. *Metallomics* **2017**, *9*, 1576-1584.
41. Lew, J.; Taylor, S. S.; Adams, J. A., Identification of a Partially Rate-Determining Step in the Catalytic Mechanism of Camp-Dependent Protein Kinase: A Transient Kinetic Study Using Stopped-Flow Fluorescence Spectroscopy. *Biochemistry* **1997**, *36*, 6717-6724.
42. Masterson, L. R.; Shi, L.; Metcalfe, E.; Gao, J.; Taylor, S. S.; Veglia, G., Dynamically Committed, Uncommitted, and Quenched States Encoded in Protein Kinase a Revealed by Nmr Spectroscopy. *Proc Natl Acad Sci U S A* **2011**, *108*, 6969-6974.
43. Gerlits, O.; Waltman, M. J.; Taylor, S.; Langan, P.; Kovalevsky, A., Insights into the Phosphoryl Transfer Catalyzed by Camp-Dependent Protein Kinase: An X-Ray Crystallographic Study of Complexes with Various Metals and Peptide Substrate Sp20. *Biochemistry* **2013**, *52*, 3721-3727.
44. Van Patten, S. M.; Fletcher, W. H.; Walsh, D. A., The Inhibitor Protein of the Camp-Dependent Protein Kinase-Catalytic Subunit Interaction. Parameters of Complex Formation. *J Biol Chem* **1986**, *261*, 5514-5523.
45. Bhatnagar, D.; Roskoski, J., R; Rosendahl, M. S.; Leonard, N. J., Adenosine Cyclic 3',5'-Monophosphate Dependent Protein Kinase: A New Fluorescence Displacement Titration Technique for Characterizing the Nucleotide Binding Site on the Catalytic Subunit. *Biochemistry* **1983**, *22*, 6310-6317.
46. Pogacic, V.; Bullock, A. N.; Fedorov, O.; Filippakopoulos, P.; Gasser, C.; Biondi, A.; Meyer-Monard, S.; Knapp, S.; Schwaller, J., Structural Analysis Identifies Imidazo[1,2-B]Pyridazines as Pim Kinase Inhibitors with *in Vitro* Antileukemic Activity. *Cancer Res* **2007**, *67*, 6916-6924.

Table of contents figure

